symmetry

MDPI

Article

Exploring the Multiplication of Resonant Modes in Off-Center-Driven Chladni Plates from Maximum Entropy States

Song-Qing Lin [1], Yu-Hsin Hsu [1], Kuan-Wei Su [1], Hsing-Chih Liang [2] and Yung-Fu Chen [1,*]

[1] Department of Electrophysics, National Yang Ming Chiao Tung University, Hsinchu 30010, Taiwan; songqinglin634.sc11@nycu.edu.tw (S.-Q.L.); yuhsin.sc10@nycu.edu.tw (Y.-H.H.); sukuanwei@nycu.edu.tw (K.-W.S.)
[2] Institute of Physics, National Yang Ming Chiao Tung University, Hsinchu 30010, Taiwan; hcliang@nycu.edu.tw
* Correspondence: yfchen@nycu.edu.tw

Abstract: In this study, the resonant characteristics of the off-center-driven Chladni plates were systematically investigated for the square and equilateral triangle shapes. Experimental results reveal that the number of the resonant modes is considerably increased for the plates under the off-center-driving in comparison to the on-center-driving. The Green's functions derived from the nonhomogeneous Helmholtz equation are exploited to numerically analyze the information entropy distribution and the resonant nodal-line patterns. The experimental resonant modes are clearly confirmed to be in good agreement with the maximum entropy states in the Green's functions. Furthermore, the information entropy distribution of the Green's functions can be used to reveal that more eigenmodes can be triggered in the plate under the off-center-driving than the on-center-driving. By using the multiplication of the resonant modes in the off-center-driving, the dispersion relation between the experimental frequency and the theoretical wave number can be deduced with more accuracy. It is found that the deduced dispersion relations agree quite well with the Kirchhoff–Love plate theory.

Keywords: Chladni patterns; vibrating plates; information entropy; geometry; Green's function

Citation: Lin, S.-Q.; Hsu, Y.-H.; Su, K.-W.; Liang, H.-C.; Chen, Y.-F. Exploring the Multiplication of Resonant Modes in Off-Center-Driven Chladni Plates from Maximum Entropy States. *Symmetry* **2024**, *16*, 1460. https://doi.org/10.3390/sym16111460

Academic Editors: Stefano Profumo and Alberto Ruiz Jimeno

Received: 1 October 2024
Revised: 28 October 2024
Accepted: 1 November 2024
Published: 3 November 2024

1. Introduction

Ernst Chladni (1756–1827) was a physicist and musician who invented an appealing experiment to demonstrate various vibration modes on a surface [1,2]. He published this experiment in his book "Entdeckungen über die Theorie des Klanges" in 1787 [3]. This experiment involved drawing a bow over a thin plate whose surface was lightly covered with sand. When the plate was bowed to reach modal resonance, the sand was caused to jump and localize on the nodal-lines, manifesting mode structures as splendid patterns [4]. Nowadays, the nodal-line patterns are called Chladni figures or Chladni patterns. Nevertheless, Chladni's demonstration was associated with earlier experiments made by Robert Hooke in 1680, who exploited a bow to vibrate a glass plate covered with some flour and observed the formation of nodal patterns [5]. However, Galileo Galilei [6], in 1632, had mentioned the observed patterns when he was scraping a brass plate with a sharp iron chisel to remove some spots from it. Scraping with the chisel repeatedly, Galilei found that it was only when the plate yielded hissing sounds that some traces of marks were left upon it. Even earlier, Leonardo da Vinci recorded this resonant phenomenon after observing how the dust on his worktable moved as he vibrated the table in the late 1400s [7].

Several different wave equations and solutions have been proposed to theoretically study the nodal-line patterns. For instance, Kirchhoff [8–10] took the effects of deformation and stresses into account to analyze the resonant modes of a circular vibrating plate. This approach was then applied to the square plate for free [9] and clamped [9,11] edges.

Nevertheless, Wah [12] found that the plates seem to behave as if they have boundary conditions between the theoretical simple support and clamped edge conditions. Furthermore, Wah [12] also noticed that it is almost impossible to simulate the results of clamped edges in the laboratory. Our research group [13] verified that the experimental resonant modes do not correspond to theoretical eigenmodes for more complex boundary conditions, and thus the nonhomogeneous Helmholtz equation should be used to solve them. Additionally, Waller [14–16] originally noticed that the nodal-line patterns at higher frequencies usually contain two or more mixed nodes due to the effects of degeneracy and damping. We also identified [17] that the formation of the resonant mode by a superposition of several degenerate or nearly degenerate eigenmodes is referred to as mode mixing. Up to now, the most successful method in the analysis of nodal-line patterns is that of the nonhomogeneous Helmholtz equation. Our group [18–20] employed the Green's function solved from the nonhomogeneous Helmholtz equation to find the response function for a vibrating wave on a thin plate as a function of the driving wave number. By substituting the theoretical wave numbers into the Green's function, the experimental nodal-line patterns have been excellently reconstructed for both the square and equilateral triangle plates [13,17–20]. More intriguingly, our research group [21] confirmed that the wave numbers corresponding to experimental resonant modes are well-related to the maximum entropy states for the square and equilateral triangle plates under the on-center-driving. Recently, the maximum entropy states have been realized as resonant modes, allowing us to arrive at a universal understanding of the relation between frequency and wave propagation within spatial boundaries under the on-center-driving [22].

In this work, we experimentally and theoretically explore the resonant phenomena of the square and equilateral triangle plates under the off-center-driving. Comparing them to the results obtained under the on-center-driving, the number of the resonant modes is found to be significantly increased for the plates under the off-center-driving. In theory, we exploit the Green's functions solved from the nonhomogeneous Helmholtz equation to analyze the experimental observations. From the theoretical reconstruction of the experimental nodal-line patterns, the resonant frequency spectrum is found to have excellent consistency with the maximum entropy states of the Green's functions. Additionally, the numerical analyses reveal that the off-center-driving can lead more eigenmodes to participate in the Green's function than the on-center-driving. Having more eigenmodes to participate in the Green's function causes the multiplication of the resonant modes in the off-center-driving. By using the off-center-driving, the increased resonant modes can be used to determine the dispersion relation between the experimental frequency and the theoretical wave number more accurately. The overall trend of the present dispersion relation is confirmed to be in good agreement with the Kirchhoff–Love plate theory [23].

2. Experimental Setup and Theoretical Model

We developed an innovative way to precisely determine the resonant frequencies at which Chladni patterns can be quickly formed, by measuring the impedance of the mechanical oscillator as a function of frequency [24]. Following our previous work [24], we determine the resonant mode frequencies by measuring the impedance of the mechanical wave driver, with and without a plate attached. Figure 1 shows the experimental setup for measuring the resonant frequency spectrum. A power amplifier was connected in series with a mechanical oscillator and a digital galvanometer. The mechanical oscillator was driven by the amplifier that generated a sinusoidal wave over the frequency range of 200–2500 Hz. The galvanometer took measurements of the impedance with a resolution of ~0.1 Hz. First of all, the measurements of the impedance were carried out without attaching the plate to the mechanical oscillator. Then, the measurements of the impedance were taken by placing the plate onto the mechanical oscillator. Two different shapes of the plates were used to explore the difference between resonant frequency spectra and nodal-line patterns between the on-center and off-center-driving. One shape is an equilateral triangle plate

with a side length of 365 mm; the other shape is a square plate with a side length of 320 mm. All plates were made with aluminum sheets of 1.0 mm thickness.

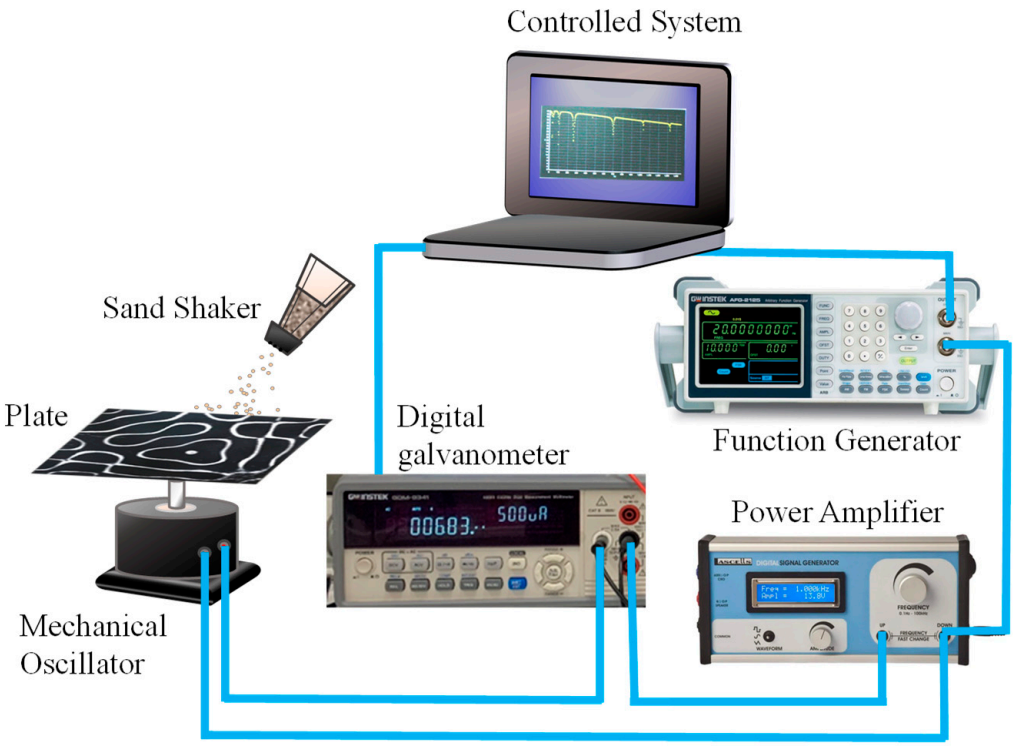

Figure 1. Experimental setup for measuring the resonant frequency spectrum and resonant patterns of a modern Chladni plate.

It has been theoretically confirmed that when the aspect ratio of the thickness to the lateral dimension for the thin plate is smaller than 0.02, the eigenmodes can be calculated by using the two-dimensional (2D) Helmholtz equation [25]. Although Rayleigh [26] noticed that the free edge boundary conditions make the problem particularly difficult, the eigenmodes can be modelled by approximating that every point of the circumference is free to move along lines that are perpendicular to the plane of the plate. In other words, the boundary condition can be simplified as the Neumann boundary condition with $\partial\psi/\partial n = 0$ on the periphery. It has been confirmed [15] that the Neumann boundary condition can be employed to successfully calculate experimental Chladni figures. Based on this success, the Neumann boundary condition with a point vibration source is used to analyze the modern Chladni figures under the on-center and off-center-driving.

The 2D Helmholtz equation for the eigenvalues k_n and eigenfunctions ψ_n with the indices of $n = 1, 2, 3 \cdots$ for the domain Ω with the boundary shape dΩ can be expressed as

$$\left(\nabla_{2D}^2 + k_n^2\right)\psi_n(\mathbf{r}) = 0. \tag{1}$$

For exploring the modern Chladni plate, we use the nonhomogeneous Helmholtz equation with a point source at $\mathbf{r}_s$ and a driving amplitude of A that is given by

$$\left(\nabla_{2D}^2 + k^2\right)\Psi(\mathbf{r}, \mathbf{r}_s; k) = A\,\delta(\mathbf{r} - \mathbf{r}_s), \tag{2}$$

Based on the property of the complete set, the eigenfunctions $\{\ \psi_n(\mathbf{r})\ \}$ $(n = 1, 2, 3 \cdots)$ can be used to expand the source function $\delta(\mathbf{r} - \mathbf{r}_s)$ and the response function $\Psi(\mathbf{r}, \mathbf{r}_s; k)$ in Equation (2). Consequently, we have

$$\delta(\mathbf{r}-\mathbf{r}_s) = \lim_{N\to\infty} \sum_{n=1}^{N} \psi_n^*(\mathbf{r}_s)\ \psi_n(\mathbf{r}), \tag{3}$$

$$\Psi(\mathbf{r},\mathbf{r}_s;k) = \lim_{N\to\infty} \sum_{n=1}^{N} a_n(\mathbf{r}_s;k)\ \psi_n(\mathbf{r}). \tag{4}$$

The coefficients $a_n(\mathbf{r}_s;k)$ in Equation (4) can be derived by substituting Equations (3) and (4) into Equation (2) and using Equation (1) for solving. The result can be obtained as

$$a_n(\mathbf{r}_s;k) = A\frac{\psi_n^*(\mathbf{r}_s)}{k^2-k_n^2}. \tag{5}$$

In fact, the response function is just proportional to the Green's function $G(\mathbf{r},\mathbf{r}_s;k)$, as given by $\Psi(\mathbf{r},\mathbf{r}_s;k) = A\ G(\mathbf{r},\mathbf{r}_s;k)$, where the Green's function is given by

$$G(\mathbf{r},\mathbf{r}_s;k) = \lim_{N\to\infty} \sum_{n=1}^{N} \frac{\psi_n^*(\mathbf{r}_s)\ \psi_n(\mathbf{r})}{k^2-k_n^2}\ . \tag{6}$$

A finite upper limit N is chosen in the numerical computation. Physically, the use of a finite limit N can be considered as a truncated basis. Nevertheless, the numerical calculation revealed that the calculated results for the entropy analyses and the nodal-line patterns can be utterly not affected when the limit N is sufficient large.

For the bipartite states, the information entropy has been employed to analyze the degree of spatial entanglement [27–30]. For the modern Chladni experiment with the on-center-driving, the information entropy distribution of the response function has been verified to be greatly useful in identifying the resonant modes [17,20]. From the Shannon theory, the information entropy distribution for the response function $\Psi(\mathbf{r},\mathbf{r}_s;k)$ can be found in terms of the coefficients $a_n(\mathbf{r}_s;k)$ to be given by [31,32]

$$S(\mathbf{r}_s;k) = -\sum_{n=1}^{N} p_n(\mathbf{r}_s;k)\ln[p_n(\mathbf{r}_s;k)], \tag{7}$$

where the probability distribution $p_n(\mathbf{r}_s;k)$ is expressed as

$$p_n(\mathbf{r}_s;k) = \frac{|a_n(\mathbf{r}_s;k)|^2}{\sum_{n=1}^{N}|a_n(\mathbf{r}_s;k)|^2}. \tag{8}$$

So far, the correspondence between the information entropy distribution and the resonant frequency spectrum is confirmed for the case with the on-center-driving. In this work, the information entropy distributions are further explored to confirm whether they are also highly associated with the resonant frequency spectra for the square and equilateral triangle plates under the off-center-driving.

The eigenfunctions and the eigenvalues for a square-shaped plate with the region in $0 \le x, y \le L$ are given by

$$\psi_{n,m}(\mathbf{r}) = \frac{2}{L}\cos\Big(\frac{n\pi}{L}x\Big)\cos\Big(\frac{m\pi}{L}y\Big), \tag{9}$$

$$k_{n,m} = \frac{\pi}{L}\sqrt{n^2+m^2}. \tag{10}$$

From Equations (5) and (8), the probability for the component $\psi_{n,m}(\mathbf{r})$ in the response function with a given upper index of N is given by

$$p_{n,m}(\mathbf{r}_s;k) = \left[\sum_{n=1}^{N}\sum_{m=1}^{N}\frac{|\psi_{n,m}(\mathbf{r}_s)|^2}{\left(k^2-k_{n,m}^2\right)^2}\right]^{-1}\frac{|\psi_{n,m}(\mathbf{r}_s)|^2}{\left(k^2-k_{n,m}^2\right)^2}. \tag{11}$$

Substituting Equation (11) into Equation (7), the information entropy can be given by

$$S(\mathbf{r}_s;k) = -\sum_{n=1}^{N}\sum_{m=1}^{N} p_{n,m}(\mathbf{r}_s;k)\ln[p_{n,m}(\mathbf{r}_s;k)]. \tag{12}$$

On the other hand, the even-symmetry eigenfunctions for the equilateral triangle plate with vertices at $(0,\ 0)$, $(L/2,\ \sqrt{3}L/2)$ and $(-L/2,\ \sqrt{3}L/2)$ are given by [33]

$$\begin{aligned}\widetilde{\psi}_{n,m}(\mathbf{r}) = \sqrt{\tfrac{16}{L^2 3\sqrt{3}}}\Big\{&\cos\left[\tfrac{2\pi}{3L}(2n-m)x\right]\cos\left(\tfrac{2\pi}{\sqrt{3}L}m\,y\right)\\ &+\cos\left[\tfrac{2\pi}{3L}(2m-n)x\right]\cos\left(\tfrac{2\pi}{\sqrt{3}L}n\,y\right)\\ &+\cos\left[\tfrac{2\pi}{3L}(n+m)x\right]\cos\left[\tfrac{2\pi}{\sqrt{3}L}(n-m)y\right]\Big\}\end{aligned} \tag{13}$$

for $m \geq 2n$. The corresponding eigenvalue is given by

$$\widetilde{k}_{n,m} = \frac{4\pi}{3L}\sqrt{n^2+m^2-n\,m}. \tag{14}$$

Similarly, the information entropy distribution for the equilateral triangle plate with an upper index of N can be given by

$$S(\mathbf{r}_s;k) = -\sum_{n=1}^{N}\sum_{m=2n}^{N} p_{n,m}(\mathbf{r}_s;k)\ln[p_{n,m}(\mathbf{r}_s;k)], \tag{15}$$

$$p_{n,m}(\mathbf{r}_s;k) = \left[\sum_{n=1}^{N}\sum_{m=2n}^{N}\frac{|\widetilde{\psi}_{n,m}(\mathbf{r}_s)|^2}{\left(k^2-\widetilde{k}_{n,m}^2\right)^2}\right]^{-1}\frac{|\widetilde{\psi}_{n,m}(\mathbf{r}_s)|^2}{\left(k^2-\widetilde{k}_{n,m}^2\right)^2}. \tag{16}$$

The information entropy can be exploited to evaluate the effective number N_{eff} of participated eigenfunctions in the response function, given by $N_{eff} = \exp[S(\mathbf{r}_s;k)]$. It has been verified that the resonant wave numbers can be properly attained from local maxima of the spectrum N_{eff} [17,20].

3. Experimental Results and Theoretical Analyses

For the equilateral triangle case, two plates were prepared to explore the difference of resonant characteristics between the on-center- and off-center-driven oscillations. As shown in Figure 2, the center position is at $(0,\ \sqrt{3}L/3)$ for the equilateral triangle plate, with vertices specified at $(0,\ 0)$, $(L/2,\ \sqrt{3}L/2)$ and $(-L/2,\ \sqrt{3}L/2)$. The plate for the off-center-driven oscillation was to set the driving position at $(0,\ \sqrt{3}L/2.72)$. Figure 3a plots the experimental results for the resonant frequency spectrum by measuring the difference of the impedance as a function of the driving frequency for the equilateral triangle plate under the on-center-driving. The resonant frequencies can be reproducibly identified from the peaks of the frequency spectrum. The corresponding nodal-line patterns for the resonant modes are also illustrated in Figure 3a. Experimental results reveal that there are nine resonant modes to be evidently obtained for the driving frequency in the range of 300–2300 Hz. On the other hand, the experimental results for the off-center-driving are depicted in Figure 3b. Comparing them to the results in Figure 3a, the number of the resonant modes can be seen to be increased more than two times. Furthermore, the resonant frequencies for the off-center-driving are significantly different to those obtained from the on-center-driving.

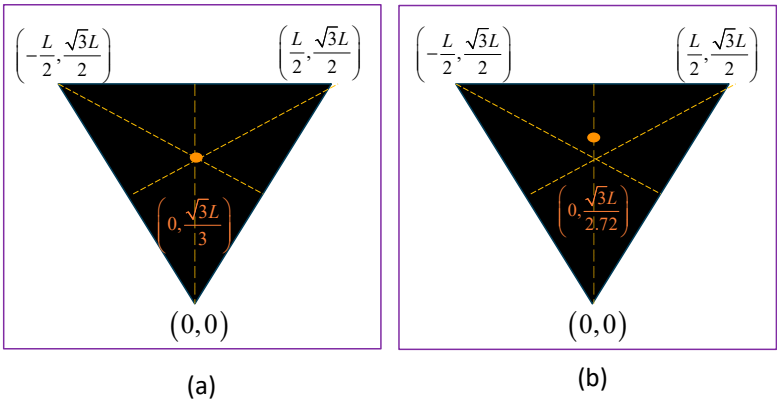

Figure 2. Coordinates for the vertices and driving position for the equilateral triangle plate: (**a**) on-center case; (**b**) off-center case.

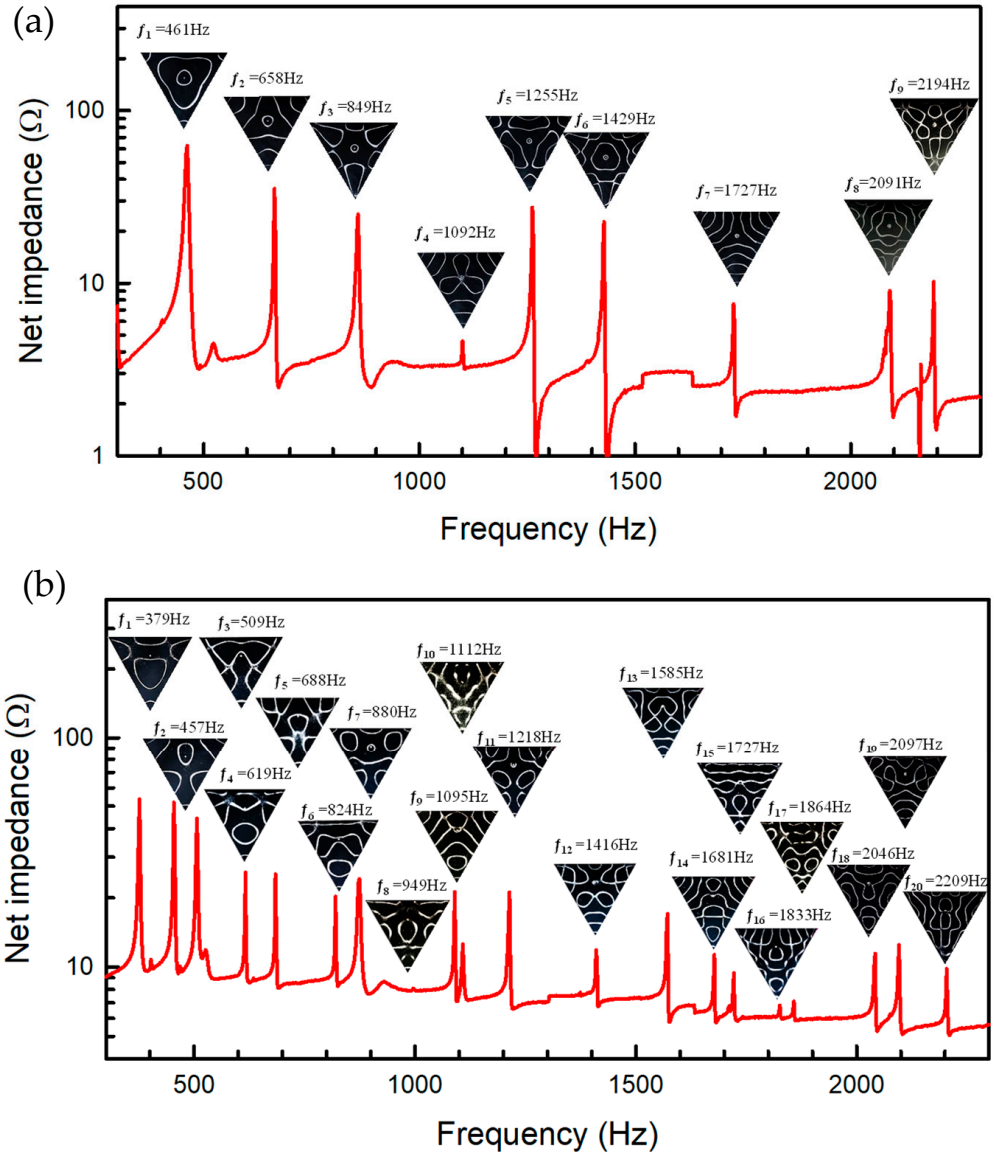

Figure 3. Resonant frequency spectrum as a function of the driving frequency for the equilateral triangle plate under (**a**) on center and (**b**) off center driving. Red lines: net impedance; insets: resonant patterns.

In theoretical analyses, the Green's function in Equation (6) is used to reconstruct the experimental nodal-line patterns for both of the on-center and off-center cases. Figure 4a,b show the calculated nodal-line patterns corresponding to the experimental results. By using Equation (16), the information entropy distribution for the equilateral triangle plate is calculated as a function of the wave number for both of the on-center and off-center cases, as shown in Figure 4a and b, respectively. From the best reconstructions of the experimental patterns, the theoretical wave numbers corresponding to resonant frequencies are marked in the information entropy distribution. It can be clearly seen that most of the resonant wave numbers are positioned near the peaks of the entropy distribution. In other words, the resonant modes almost correspond to the Green's functions with maximal entropy states. More importantly, the multiplication of the resonant modes can also be manifested from the information entropy distribution. This finding indicates that the maximum entropy states play a critical role not only in the on-center but also the off-center cases. To be brief, the peaks of the information entropy distribution can be exploited to determine the number of the resonant modes, as well as the resonant wave numbers.

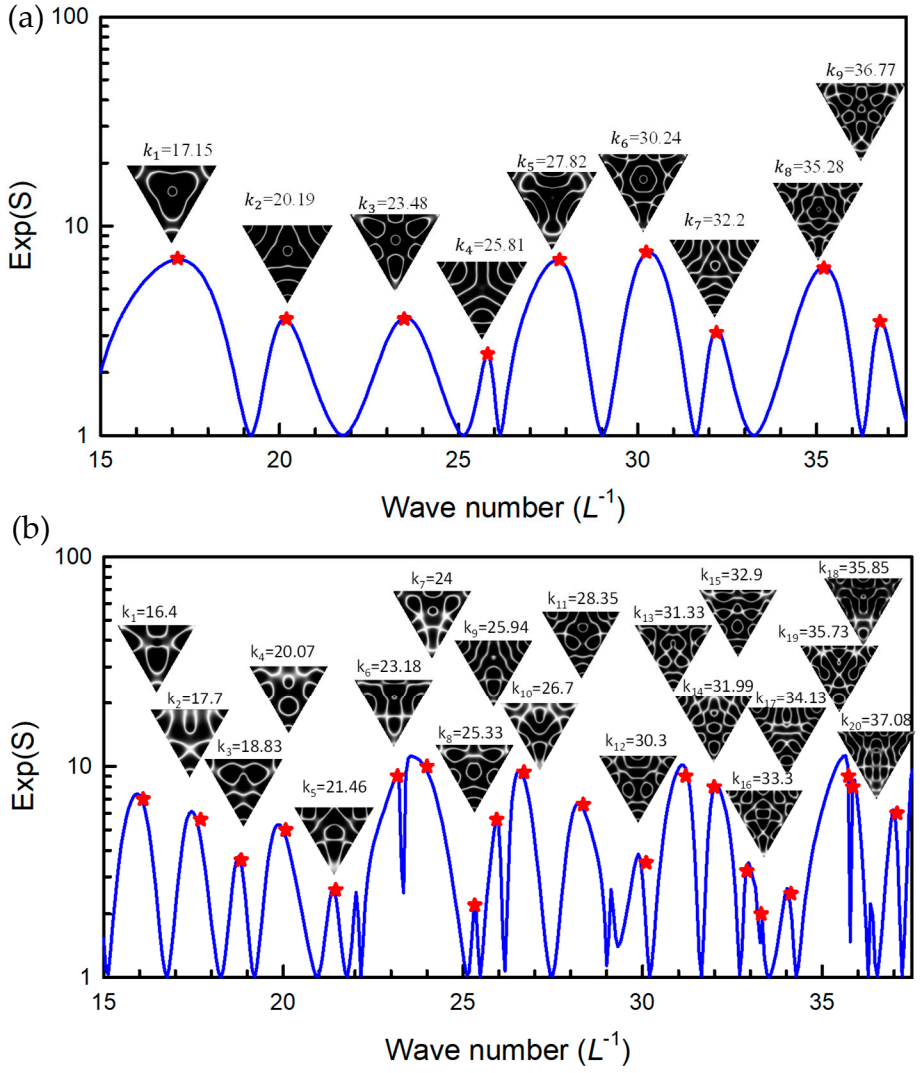

Figure 4. Calculated results for information entropy distribution as a function of wave number and nodal-line patterns corresponding to experimental observations in Figure 3 for (**a**) on-center and (**b**) off-center cases. Blue lines: net impedance; red stars: resonant points; insets: resonant patterns.

4. Discussion

The multiplication of the resonant modes can be comprehended from the effective number of the participated eigenmodes in the Green's function. From Equation (16), the probability coefficients of the participated eigenmodes in the Green's function are proportional to $\left| \widetilde{\psi}_{n,m}(\mathbf{r}_s) \right|^2$. For the on-center-driving, the source point is at $\mathbf{r}_s = (0,\ \sqrt{3}L/3)$, which leads the relative probability coefficients to be given by

$$\left| \widetilde{\psi}_{n,m}(\mathbf{r}_s) \right|^2 = \left| \sqrt{\frac{16}{L^2 3\sqrt{3}}} \left\{ \cos\left(\frac{2\pi}{3}m\right) + \cos\left(\frac{2\pi}{3}n\right) + \cos\left[\frac{2\pi}{3}(n-m)\right] \right\} \right|^2 \quad (17)$$

From Equation (17), it can be verified that the probability coefficients of the eigenstates vanish when the indices (m,n) satisfy $m - n = 3s + 1$ for s to be any positive integer. On the other hand, the source point for the off-center-driving is at $\mathbf{r}_s = (0,\ \sqrt{3}L/2.72)$, which leads the relative probability coefficients to be given by

$$\left| \widetilde{\psi}_{n,m}(\mathbf{r}_s) \right|^2 = \left| \sqrt{\frac{16}{L^2 3\sqrt{3}}} \left\{ \cos\left(\frac{2\pi}{2.72}m\right) + \cos\left(\frac{2\pi}{2.72}n\right) + \cos\left[\frac{2\pi}{2.72}(n-m)\right] \right\} \right|^2 \quad (18)$$

All of the probability coefficients of the eigenstates can be confirmed to be nonzero. Figure 5a,b depict the relative probability coefficients calculated with Equations (17) and (18), respectively, for the indices in the range of $1 \leq m, n \leq 20$. It can be clearly seen that the off-center-driving can lead more eigenmodes to participate in the Green's function than the on-center case. The more eigenmodes that participate in the Green's function, the more resonant modes that can be produced.

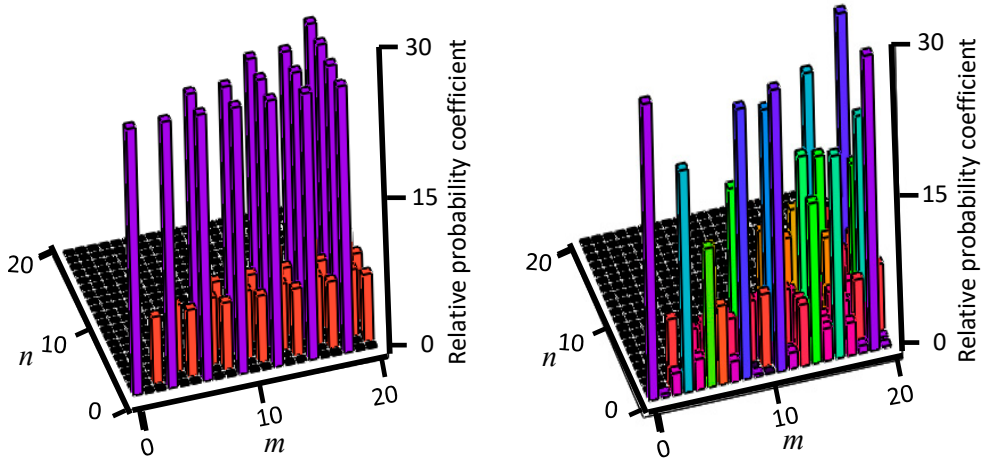

(a) on-center driving (b) off-center driving

Figure 5. Relative probability coefficients calculated with Equations (17) and (18), respectively, for the indices in the range of $1 \leq m, n \leq 20$ for (**a**) on-center-driving and (**b**) off-center-driving. Colors for manifesting amplitudes.

The good agreement between the resonant modes and the maximum entropy states can be traced back to the principle of energy equipartition in statistical mechanics. The applications of the maximum entropy principle have included the maximum emission of the multimode laser systems [34], the self-organization of the complex systems [35], the wave localization of the disordered systems [36] and the phase transitions of open quantum systems [37]. In this work, we clearly demonstrate that the maximum entropy principle can be applied to the modern Chladni plates, not only for the on-center-driving, but also

for general off-center cases. This demonstration paves an intriguing way for using the off-center-driving to develop novel applications related to the vibrating plates.

From the analyses of the resonant nodal-line patterns, the dispersion relation between the experimental frequency f and the theoretical wave number k can be obtained. Since the off-center-driving can significantly increase the number of the resonant modes, the dispersion relation between f and k can be deduced more accurately. Based on the Kirchhoff–Love plate theory [23], the dispersion relation between the frequency and wave number for the flexural wave of the plate can be derived as

$$f(k) = \sqrt{\frac{D}{\rho h}} \frac{1}{2\pi} k^2 \tag{19}$$

where h is the thickness of the plate, ρ is the mass density, and D is the flexural rigidity. The flexural rigidity is given by

$$D = \frac{Eh^3}{12(1-\nu^2)} \tag{20}$$

E is the Young's modulus and ν is the Poisson ratio. Equation (19) can be simply expressed as $f(k) = A\,k^2$, where A is the proportional coefficient. The theoretical value of the coefficient A can be calculated from the properties of aluminum, as follows [38]: E = 68 GPa, ν = 0.33, ρ = 2700 kg/m^3 and h = 1 mm. As a result, the theoretical value is $A = 0.244$. Figure 6 plots the theoretical dispersion relation and the present results deduced from the correspondence between the resonant frequencies f and the resonant wave numbers k. The overall trend between the theoretical and present results can be seen to be rather consistent. For the best fitting to the present results, the proportional coefficient is 0.215, which is slightly smaller than the theoretical value. The discrepancy between the theoretical and present results may come from the assumption and approximation in deriving Equation (19).

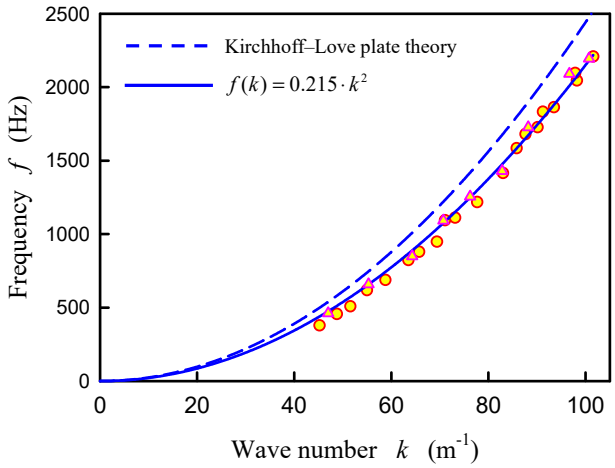

Figure 6. Theoretical dispersion relation and the present results deduced from the correspondence between the resonant frequencies f and the resonant wave numbers k. Symbols: triangles obtained from on-center driving; circles obtained from off-center driving.

Finally, we further confirm the practicability of the maximum entropy states by exploring the square plate under the off-center-driving. For the square plate with the vertices at $(0,\ 0)$, $(0,\ L)$, $(\ L, 0)$ and $(L,\ L)$, the center position can be found to be at $(L/2,\ L/2)$. For the investigation of the off-center-driving, the mechanical oscillator was set at $(4L/7,\ 3L/7)$, along the diagonal line. The experimental results for the resonant frequency spectrum and the resonant nodal-line patterns for this off-center-driving square plate are shown in Figure 7. The number of the resonant modes for the off-center-driving is also found to be considerably increased, similar to the results observed in the equilateral triangle plate.

Figure 8 shows the calculated results for the information entropy distribution, corresponding to the experimental case. The theoretical wave numbers marked in the information entropy distribution to correspond to resonant modes are obtained by using the Green's function to reconstruct the experimental nodal-line patterns. Once again, most of the resonant wave numbers can be clearly seen to be well-localized near the peaks of the entropy distribution. This further confirmation indicates that the maximum entropy states can be exploited to analyze the number of the resonant modes, as well as the resonant nodal-line patterns for any driving positions.

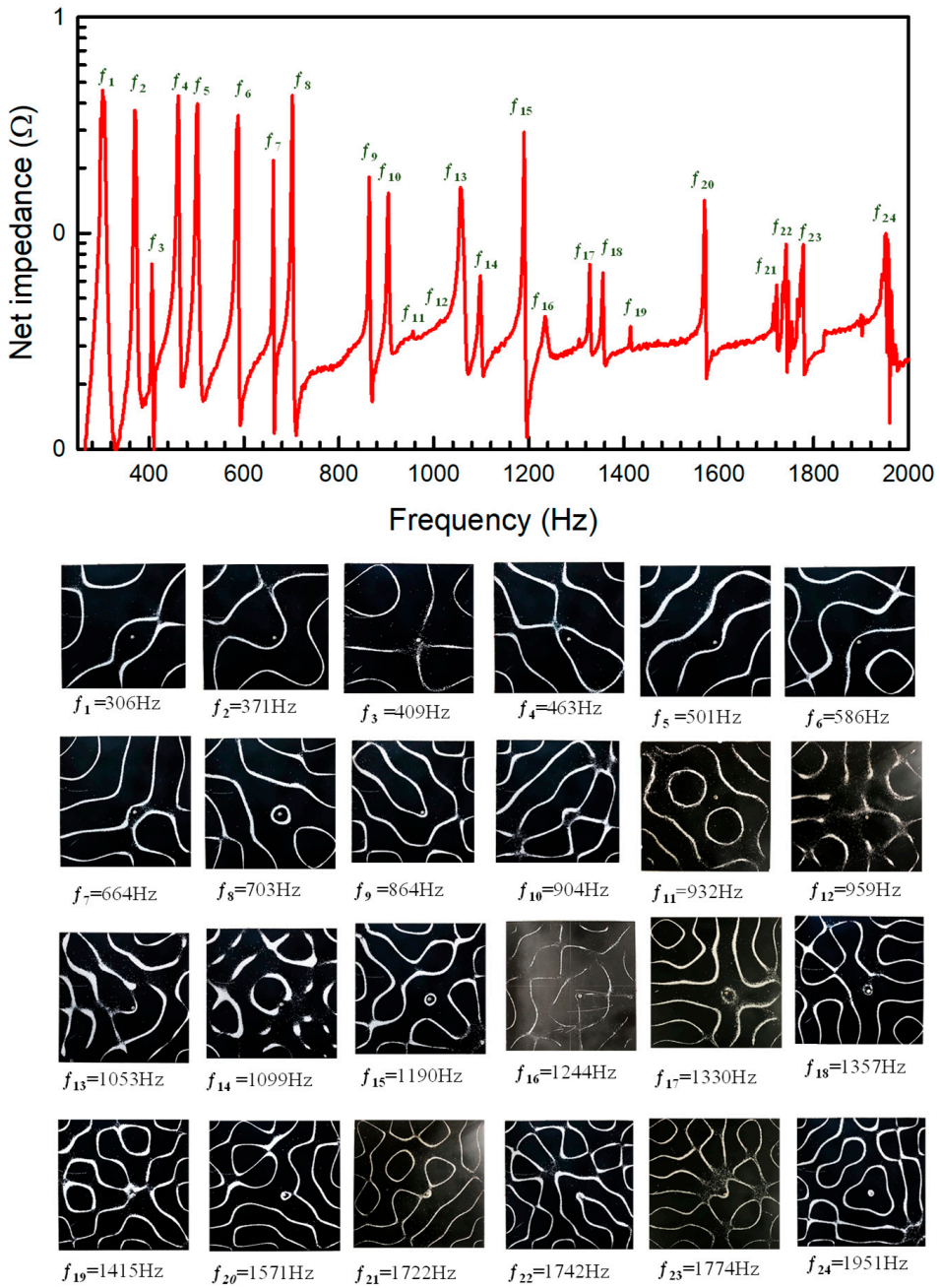

Figure 7. Experimental results for the resonant frequency spectrum and the resonant nodal-line patterns for this off-center-driving square plate.

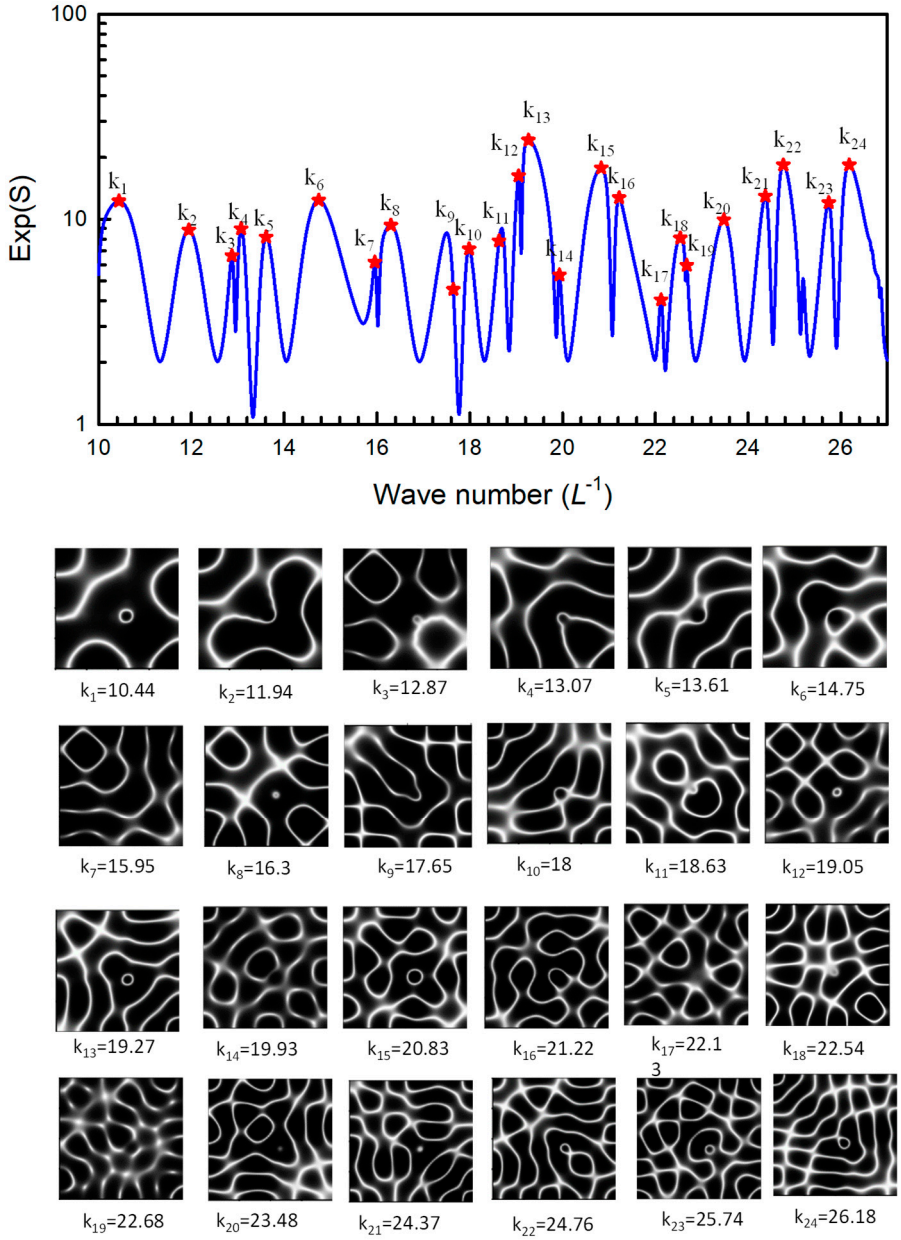

Figure 8. Calculated results for the information entropy distribution corresponding to the experimental result in Figure 7. Wave numbers marked in the information entropy distribution obtained from the best reconstructions of experimental nodal-line patterns with the Green's functions. Red stars: resonant points.

5. Conclusions

We have experimentally and theoretically studied the resonant characteristics of the off-center-driven Chladni plates for the square and equilateral triangle shapes. We experimentally found that the number of the resonant modes under the off-center-driving is substantially increased in comparison to the plate under the on-center-driving. The origin of appearing to have more resonant modes under the off-center-driving is confirmed to be from the result that more eigenmodes can be excited to participate in the response function. Additionally, we theoretically used the Green's functions of the nonhomogeneous Helmholtz equation to analyze the experimental nodal-line patterns. It is confirmed that the experimental resonant modes are nicely consistent with the maximum entropy states in the information entropy distribution of the Green's functions. Furthermore, we exploited the multiplication of the resonant modes in the off-center-driving to analyze

the dispersion relation between the experimental frequency and the theoretical wave number. The analyzed dispersion relations are found to be in good agreement with the theorical formula. The present finding may pave an insight into some applications, such as biomedical engineering to harmonize organic systems. On the other hand, the present exploration provides a way to reduce information dispersion in systems that interact from the atomic level. It is worthwhile to mention that the maximum entropy principle is expected to be appliable to the polygon plates, and not only the present showing cases. However, the challenge of exploring the generation for polygons consists of the lack of analytical mathematical forms for the eigenmodes. The further exploration of polygon plates is thus underway.

Author Contributions: Conceptualization, Y.-F.C.; validation, S.-Q.L. and Y.-H.H.; formal analysis, S.-Q.L. and H.-C.L.; resources, Y.-H.H. and K.-W.S.; writing—original draft preparation, Y.-F.C.; writing—review and editing, S.-Q.L., Y.-H.H. and Y.-F.C.; supervision, Y.-F.C. All authors have read and agreed to the published version of the manuscript.

Funding: This work is supported by the National Science and Technology Council of Taiwan (contract number 112-2112-M-A49-022-MY3).

Data Availability Statement: All data reported in the paper are presented in the main text. Any other data will be provided on request.

Conflicts of Interest: The authors declare no conflicts of interest.

References

1. Chladni, E.F.F. *Treatise on Acoustics: The 1st Comprehensive English Translation of E.F.F. Chladni's Traité d'Acoustique*; Springer: Berlin/Heidelberg, Germany, 2015.
2. Musielak, D.E. *Prime Mystery: The Life and Mathematics of Sophie Germain Paperback*; Author House: Bloomington, IN, USA, 2015.
3. Chladni, E.F.F. *Entdeckungen über Die Theorie des Klanges*; Bey Weidmannserben und Reich: Leipzig, Germany, 1787.
4. Chladni, E.F.F. *Neue Beitruge zur Akustik*; Breitkopf und Hartel: Leipzig, Germany, 1817.
5. Andrade, E.N.D.C. Wilkins Lecture—Robert Hooke. *Proc. R. Soc. Lond. Ser. B Biol. Sci.* **1997**, *137*, 153–187.
6. Galilei, G. *Dialogues Concerning Two New Sciences*; Crew, H.; de Salvio, A., Translators; Macmillan: London, UK, 1914; pp. 209–221.
7. Kovacic, I.; Kanovic, Z. Chladni Plate in Anechoic Chamber: Symmetry in Vibrational and Acoustic Response. *Symmetry* **2023**, *15*, 1748. [CrossRef]
8. Kirchhoff, G. Uber das Gleichgewicht und die Bewegung einer elastischen Scheibe. *J. Reine Angew. Math.* **1850**, *40*, 51–88.
9. Rayleigh, J.W.S. (Ed.) Vibrations of Plates. In *The Theory of Sound*; Macmillan and Co.: London, UK, 1877; Volume 1, Chapter 10, pp. 203–326.
10. Leissa, A.W. (Ed.) *Vibration of Plates*; Ohio State University: Columbus, OH, USA, 1969.
11. Timoshenko, S. *Vibration Problems in Engineering*, 3rd ed.; D. Van Nostrand Company, Inc.: Princeton, NJ, USA, 1961.
12. Wah, T. Vibration of Circular Plates. *J. Acoust. Soc. Am.* **1962**, *34*, 275–281. [CrossRef]
13. Tuan, P.H.; Wen, C.P.; Yu, Y.T.; Liang, H.C.; Huang, K.F.; Chen, Y.F. Exploring the distinction between experimental resonantmodes and theoretical eigenmodes: From vibrating plates to laser cavities. *Phys. Rev. E* **2014**, *89*, 022911. [CrossRef] [PubMed]
14. Waller, M.D. Vibrations of free circular plates. Part 2: Compounded normal modes. *Proc. Phys. Soc.* **1938**, *50*, 77–82. [CrossRef]
15. Waller, M.D. Vibrations of free square plates: Part I. Normal vibrating modes. *Proc. Phys. Soc.* **1939**, *51*, 831–844. [CrossRef]
16. Waller, M.D. Vibrations of free square plates: Part II, compounded normal modes. *Proc. Phys. Soc.* **1940**, *52*, 452–455. [CrossRef]
17. Tuan, P.H.; Wen, C.P.; Chiang, P.Y.; Yu, Y.T.; Liang, H.C.; Huang, K.F.; Chen, Y.F. Exploring the resonant vibration of thin plates: Reconstruction of Chladni patterns and determination of resonant wave numbers. *J. Acoust. Soc. Am.* **2015**, *137*, 2113–2123. [CrossRef]
18. Tuan, P.H.; Tung, J.C.; Liang, H.C.; Chiang, P.Y.; Huang, K.F.; Chen, Y.F. Resolving the formation of modern Chladni figures. *EPL Europhys. Lett.* **2015**, *111*, 64004. [CrossRef]
19. Tuan, P.H.; Liang, H.C.; Tung, J.C.; Chiang, P.Y.; Huang, K.F.; Chen, Y.F. Manifesting the evolution of eigenstates from quantum billiards to singular billiards in the strongly coupled limit with a truncated basis by using RLC networks. *Phys. Rev. E* **2015**, *92*, 062906. [CrossRef] [PubMed]
20. Tuan, P.H.; Lai, Y.H.; Wen, C.P.; Huang, K.F.; Chen, Y.F. Point-driven modern Chladni figures with symmetry breaking. *Sci. Rep.* **2018**, *8*, 10844. [CrossRef]
21. Shu, Y.-H.; Tseng, Y.-C.; Lai, Y.-H.; Yu, Y.-T.; Huang, K.-F.; Chen, Y.-F. Exploring the Origin of Maximum Entropy States Relevant to Resonant Modes in Modern Chladni Plates. *Entropy* **2022**, *24*, 215. [CrossRef]
22. Val Baker, A.; Csanad, M.; Fellas, N.; Atassi, N.; Mgvdliashvili, I.; Oomen, P. Exploration of Resonant Modes for Circular and Polygonal Chladni Plates. *Entropy* **2024**, *26*, 264. [CrossRef]

23. Leissa, A.W. *Vibration of Plates*; Acoustical Society of America: New York, NY, USA, 1993; pp. 1–345.
24. Tseng, Y.C.; Hsu, Y.H.; Lai, Y.H.; Yu, Y.T.; Liang, H.C.; Huang, K.F.; Chen, Y.F. Exploiting modern Chladni plates to analogously nanifest the point interaction. *Appl. Sci.* **2021**, *11*, 10094. [CrossRef]
25. Ventsel, E.; Krauthammer, T. *Thin Plates and Shells*; Marcel Dekker: New York, NY, USA, 2004; pp. 1–14.
26. Lord Rayleigh. Theory of Sound. Dover: New York, NY, USA, 1945; pp. 367–380.
27. Ekert, A.; Knight, P.L. Entangled quantum systems and the Schmidt decomposition. *Amer. J. Phys.* **1995**, *63*, 415. [CrossRef]
28. Law, C.K.; Eberly, J.H. Analysis and Interpretation of High Transverse Entanglement in Optical Parametric Down Conversion. *Phys. Rev. Lett.* **2004**, *92*, 127903. [CrossRef] [PubMed]
29. Law, C.K.; Walmsley, I.A.; Eberly, J.H. Continuous Frequency Entanglement: Effective Finite Hilbert Space and Entropy Control. *Phys. Rev. Lett.* **2000**, *84*, 5304. [CrossRef] [PubMed]
30. Fedorov, M.V.; Miklin, N.I. Schmidt modes and entanglement. *Contemp. Phys.* **2014**, *55*, 94–109. [CrossRef]
31. Shannon, C.E. Prediction and entropy of printed English. *Bell Syst. Tech. J.* **1951**, *30*, 50–60. [CrossRef]
32. Jaynes, E.T. Information theory and statistical mechanics. *Phys. Rev.* **1957**, *106*, 602–630. [CrossRef]
33. Práger, M. Eigenvalues and eigenfunctions of the Laplace operator on an equilateral triangle. *Appl. Math.* **1998**, *43*, 311–320. [CrossRef]
34. Tang, C.L.; Statz, H. Maximum-emission principle and phase locking in multimode lasers. *J. Appl. Phys.* **1967**, *38*, 2963–2968. [CrossRef]
35. Haken, H. *Information and Self-Organization: A Macroscopic Approach to Complex Systems*; Springer: Berlin/Heidelberg, Germany, 2006.
36. Heller, E.J. Quantum localization and the rate of exploration of phase space. *Phys. Rev. A* **1987**, *35*, 1360–1370. [CrossRef]
37. Jung, C.; Müller, M.; Rotter, I. Phase transitions in open quantum systems. *Phys. Rev. E* **1999**, *60*, 114–131. [CrossRef] [PubMed]
38. Van Vlack, L.H. *Elements of Material Science and Engineering*; Addison-Wesley: Boston, MA, USA, 1980.